AIP | The Journal of Chemical Physics

Potential energy surfaces for the interaction of BH(X 1Σ+,A 1Π) with Ar and a theoretical investigation of the stretchbend levels of the ArBH(A) van der Waals molecule

Millard H. Alexander, Susan Gregurick, and Paul J. Dagdigian

Citation: The Journal of Chemical Physics **101**, 2887 (1994); doi: 10.1063/1.468431
View online: http://dx.doi.org/10.1063/1.468431
View Table of Contents: http://scitation.aip.org/content/aip/journal/jcp/101/4?ver=pdfcov
Published by the AIP Publishing

Articles you may be interested in

Theoretical study of the interaction of AlH(X 1Σ+,A 1Π) with Ar: Potential energy surfaces and bend–stretch levels of the ArAlH(X,A) van der Waals complex
J. Chem. Phys. **102**, 2413 (1995); 10.1063/1.468672

Potential energy surfaces for the interaction of CH(X 2Π,B 2Σ−) with Ar and an assignment of the stretch bend levels of the ArCH(B) van der Waals molecule
J. Chem. Phys. **101**, 4547 (1994); 10.1063/1.467442

Observation and characterization of the ArBH(X 1Σ+,A 1Π) van der Waals complex through fluorescence excitation spectroscopy
J. Chem. Phys. **101**, 2903 (1994); 10.1063/1.467603

Stretch–bend coupling between van der Waals modes in the S 1 state of substituted benzene–Ar1 complexes
J. Chem. Phys. **91**, 752 (1989); 10.1063/1.457127

van der Waals bond stretch and bend frequencies in the molecules tetrazine–X (X=Xe, Kr, and Ar)
J. Chem. Phys. **88**, 6082 (1988); 10.1063/1.454501

This article is copyrighted as indicated in the article. Reuse of AIP content is subject to the terms at: http://scitation.aip.org/termsconditions. Downloaded to IP: 128.114.34.22 On: Mon, 01 Dec 2014 02:28:05

Potential energy surfaces for the interaction of BH($X\ ^1\Sigma^+$,$A\ ^1\Pi$) with Ar and a theoretical investigation of the stretch-bend levels of the ArBH(A) van der Waals molecule

Millard H. Alexander and Susan Gregurick
Department of Chemistry and Biochemistry, University of Maryland, College Park, Maryland 20742

Paul J. Dagdigian
Department of Chemistry, The Johns Hopkins University, Baltimore, Maryland 21218

(Received 25 February 1994; accepted 28 April 1994)

New multireference, configuration-interaction potential energy surfaces are reported for the interaction of Ar with the BH radical in its ground ($X\ ^1\Sigma^+$) and first excited ($A\ ^1\Pi$) electronic states. These potential energy surfaces are then used with an adiabatic bender model for the calculation of the vibrational energy levels of the ArBH van der Waals complex in its ground and first excited singlet electronic states. Comparison of vibrational energies calculated using this adiabatic bender model with computed exact vibrational energies indicates that the former provides a very useful description of the bound levels of the ArBH complex. A qualitative discussion of the expected features in the $A\ ^1\Pi - X\ ^1\Sigma^+$ electronic spectrum of ArBH is also presented, to facilitate comparison with the experimental ArBH spectrum reported in the following paper [E. Hwang and P. J. Dagdigian, following paper, J. Chem. Phys. **101**, 2903 (1994)]. The most strongly bound ArBH(A) levels, with Ar–BH separations less than in the ground state ArBH(X) complex, correspond to motion described primarily by the more attractive $V_{A''}$ potential energy surface and to a helicopterlike internal motion of the BH moiety. For the more weakly bound states supported by higher bender curves, the vibrational motion cannot be described as occurring on either the $V_{A''}$ or $V_{A'}$ potential energy surfaces separately.

I. INTRODUCTION

There has been considerable recent interest, both experimental as well as theoretical, in van der Waals complexes of argon with diatomic free-radical hydrides.[1] A particularly successful example is the ArOH($X\ ^2\Pi$,$A\ ^2\Sigma^+$) complex. Here the *ab initio* correlated electron pair[2,3] approximation (CEPA) potential energy surfaces (PES's) of Degli–Esposti and Werner[4] have been used to interpret the electronic spectrum of the complex, which occurs near the $A\ ^2\Sigma^+ \leftarrow X\ ^2\Pi$ transition in the isolated OH radical.[5–10] These *ab initio* PES's provided an invaluable template for the subsequent development of phenomenological PES's both for the ground[11–13] [ArOH($X\ ^2\Pi$)] and excited[14–16] [ArOH($A\ ^2\Sigma^+$)] electronic states of the complex.

The electronic spectra of complexes of several other first-row hydrides with argon have recently been reported. Lester and co-workers[17] observed a number of bands of the ArNH complex, in the region of the (0,0) band of the $c\ ^1\Pi \leftarrow a\ ^1\Delta$ transition in the isolated NH radical. The interpretation of the spectrum is being aided by the availability of multireference, configuration-interaction PES's of Jansen and Hess[18] for ArNH($a\ ^1\Delta$) and of Alexander *et al.*[19] for ArNH($c\ ^1\Pi$). A complication in the assignment of the ArNH spectrum is the small anisotropy of the ArNH($a\ ^1\Delta$) PES's, which leads to sets of nearly isoenergetic bender levels. Similar spectroscopic studies of the ArCH complex, in the region of the (0,0) and (1,0) bands of the CH $B\ ^2\Sigma^- \leftarrow X\ ^2\Pi$ transition, have been reported by Lemire *et al.*[20] In the accompanying article[21] the electronic spectrum of the ArBH van der Waals complex in the region of the BH $A\ ^1\Sigma^+ \leftarrow X\ ^1\Pi$ (0,0) band is reported.

The ArBH and ArNH complexes represent the first examples of complexes involving open-shell *singlet* diatomic free radicals. Hence, complications due to the presence of an unpaired electron spin are avoided.[11,22] Nevertheless, one difficulty in understanding the pattern of the observed vibrational levels in these singlet spin multiplicity complexes, in particular for ArBH($A\ ^1\Pi$) and ArNH($c\ ^1\Pi$), is the large difference in the interaction energies when the unpaired π electron lies in or perpendicular to the triatomic plane. In theoretical treatments[11,23,24] of complexes of argon with other diatoms in degenerate electronic states, e.g., OH($X\ ^2\Pi$) and NO($X\ ^2\Pi$), this difference potential could be assumed to be a relatively small perturbation.

To provide a theoretical framework with which to interpret the ArBH spectrum, we present here multireference, configuration-interaction calculations of the PES's for the interaction of Ar with the BH radical in its ground ($X\ ^1\Sigma^+$) and first excited ($A\ ^1\Pi$) electronic states. These potential energy surfaces are then used in an adiabatic analysis, as well as a full variational calculation, of the rovibronic levels of the ArBH van der Waals complex in its ground and first excited singlet electronic states. These calculations lead into a qualitative discussion of the pattern of bend-stretch energy levels of the ArBH(A) complex. Some broad implications for the $A\ ^1\Pi - X\ ^1\Sigma^+$ electronic spectrum of the ArBH complex are then presented; a more detailed comparison of the theoretical predictions with experimental observations is deferred until the following paper.[21]

This article is copyrighted as indicated in the article. Reuse of AIP content is subject to the terms at: http://scitation.aip.org/termsconditions. Downloaded to IP: 128.114.34.22 On: Mon, 01 Dec 2014 02:28:05

 0021-9606/94/101(4)/2887/16/$6.00 © 1994 American Institute of Physics

II. QUALITATIVE DISCUSSION OF ENERGY LEVELS

The nominal electron occupancies of the BH molecule in the $X\ ^1\Sigma^+$ and $A\ ^1\Pi$ states are $1\sigma^2 2\sigma^2 3\sigma^2$ and $1\sigma^2 2\sigma^2 3\sigma 1\pi$, respectively. Approach of a spherical partner to the BH molecule in the X state will give rise to a single, closed-shell state of A' reflection symmetry (in C_s geometry). Consequently, the ArBH bending and stretching motion can be interpreted with the theoretical treatments already developed and applied to a number of van der Waals complexes involving close-shell diatoms.[25–29] By contrast, the presence of two singly filled orbitals in the excited BH $A\ ^1\Pi$ electronic state introduces an additional complexity. The cylindrical $^1\Pi$ degeneracy of the BH molecule in the A state will be lifted by approach of a collision partner. This will give rise to an additional two electronic states of A' and A'' symmetry.[30–35] In contrast to other complexes involving diatoms in Π electronic states, such as ArOH($X\ ^2\Pi$) (Refs. 4 and 11) and HFNO($X\ ^2\Pi$) (Ref. 22) our *ab initio* calculations, to be described here, indicate that the difference in the ArBH($A\ ^1\Pi$) A' and A'' PES's is too large to be accurately accounted for by a perturbation treatment.[23]

Consequently, we present here a more general framework for the discussion of the qualitative features of the rovibrational energy levels of a complex involving a diatom in a $^1\Pi$ electronic state, even in a regime where a perturbation treatment would be slowly convergent. Since the matrix elements of the interaction potential are quite similar for a diatom in both $^1\Pi$ and $^1\Delta$ electronic states, we generalize the treatment below to both types of states, in order that the present treatment can be used in a subsequent analysis[19] of the electronic spectrum of the ArNH complex.[17]

As discussed clearly by Hutson and co-workers in their general treatment of atom-diatom complexes,[23,29] the rovibronic wave functions of the ArBH complex can be expanded in a product basis of functions describing the electronic rotational motion of the BH moiety, the orbital (end-over-end) motion of Ar atom with respect to BH, and the vibrational motion of Ar with respect to the BH. Here we explicitly neglect the vibrational motion of the BH moiety. This basis is identical to that used in the description of unbound (scattering) interactions between a noble gas atom and a diatomic molecule in a state of $^1\Pi$ (Refs. 34–36) or $^1\Delta$ (Ref. 37) symmetry. We thus write

$$\Psi^{JM}=(1/R)\sum_{jl\epsilon} C^{JM}_{jl\epsilon}(R)|jl\epsilon;JM\rangle. \tag{1}$$

Here J designates the total angular momentum with space fixed projection M, l designates the orbital (end-over-end) angular momentum, and j and ϵ designate the angular momentum and e/f symmetry[38] index of the Hund's case (a) states of the $A\ ^1\Pi$ electronic state of the BH molecule [$\epsilon=+1$ for the e labeled, and -1 for the f labeled, Λ doublet states].

In Eq. (1) the functions $|jl\epsilon;JM\rangle$ are defined as

$$|jl\epsilon;JM\rangle=\sum_{m_j m_l}(jm_j lm_l|JM)Y_{lm_l}(\hat{R})\psi_{jm_j\epsilon}(\hat{r}), \tag{2}$$

where $(\cdots|\cdots)$ is a Clebsch–Gordan coefficient,[39] Y_{lm_l} is a spherical harmonic,[39] and $\hat{R}=(\theta,\phi)$ and $\hat{r}=(\beta,\alpha)$ designate the space-frame orientations of $\bar{R}$, the vector connecting the Ar atom and the diatom center of mass, and $\bar{r}$, the diatom (BH) internuclear axis. The symmetrized Hund's case (a) wave functions $\psi_{jm_j\epsilon}(\hat{r})$ can be written as

$$\psi_{jm_j\epsilon}(\hat{r})=2^{-1/2}[(2j+1)/4\pi]^{1/2}[D^{j*}_{m_j,\Lambda}(\alpha,\beta,0)|\Lambda\rangle + \epsilon D^{j*}_{m_j,-\Lambda}(\alpha,\beta,0)|-\Lambda\rangle], \tag{3}$$

where D^j_{mn} is a rotation matrix element. Here $|\Lambda\rangle$ designates the electronic wave function with Λ being the projection of the orbital angular momentum along the diatomic axis. The third Euler angle γ in Eq. (3) has been set to zero without loss of generality.[40,41] With this choice of γ, the diatom-fixed y axis lies in the plane of rotation. Because the parity of the $\psi_{jm_j\epsilon}(\hat{r})$ functions is $\epsilon(-1)^j$ (Refs. 36 and 38) and the inversion symmetry of the spherical harmonics is $(-1)^l$ (Ref. 41), the total parity ($\pm$) of the $|jl\epsilon;JM\rangle$ functions is $\epsilon(-1)^{j+l}$.

The expansion coefficients $C^{JM}_{jl\epsilon}(R)$ satisfy the standard close-coupled (CC) equations.[29,35,42] In matrix notation these are

$$\left(\frac{d^2}{dR^2}-W(R)\right)C^{JM}(R)=0, \tag{4}$$

where

$$W(R)\equiv\frac{l(l+1)}{2\mu R^2}-k^2+\frac{2\mu}{\hbar^2}V(R), \tag{5}$$

Here $l(l+1)$ and k^2 designate the diagonal matrices of the orbital angular momentum and wave vectors of the individual coupled channels, and $V(R)$ is the full matrix of the interaction potential(s). The elements of the k^2 vector are defined by

$$k^2_{j\epsilon}=(2\mu/\hbar^2)(E-E_{j\epsilon}). \tag{6}$$

In Eq. (6), μ is the Ar–BH reduced mass, E is the total energy and $E_{j\epsilon}$ designates the internal energy of the $|j\epsilon\rangle$ state of the diatomic hydride. The explicit form of the full potential matrix in the SF $|jl\epsilon;JM\rangle$ basis has been given previously[35] for the case of a diatomic molecule in a $^1\Pi$ electronic state.

The expansion used in Eqs. (1) and (2) involves space-fixed (SF) orbital and molecular angular momentum states. Equivalently, one can use states in which the angular momentum refers to the body-fixed (BF) frame, an approach advocated years ago in the quantum treatment of molecular collisions[43–45] and, more recently, in the study of atom-diatom van der Waals molecules.[29,46] We define the BF frame by the orientation of $\bar{R}$. In this case the expansion in Eq. (1) becomes

$$\Psi^{JM}=(1/R)\sum_{jP\epsilon} C^{JM}_{jP\epsilon}(R)|jP\epsilon;JM\rangle, \tag{7}$$

where, consistent with the notation of Dubernet *et al.*,[23] we use P to denote the body frame projection of j. Since the

This article is copyrighted as indicated in the article. Reuse of AIP content is subject to the terms at: http://scitation.aip.org/termsconditions. Downloaded to IP: 128.114.34.22 On: Mon, 01 Dec 2014 02:28:05

orbital angular momentum vector $\mathbf{l}$ must be perpendicular to the triatomic plane, it follows that P is also the projection of the total angular momentum $\mathbf{J}$ along $\bar{R}$.

The transformation between the body- and space-frame basis is diagonal in j and ϵ and given by (see the Appendix)

$$|jP\epsilon;JM\rangle=\sum_l (-1)^{j-l+P}(2l+1)^{1/2} \times\begin{pmatrix} j & l & J \\ P & 0 & -P \end{pmatrix}|jl\epsilon;JM\rangle, \quad (8)$$

where (:::) is a $3j$ symbol.[39] Note (see the Appendix) that the phase factor differs from that given by Hutson.[29] In Eq. (8), the BF functions can also be expressed as

$$|jP\epsilon;JM\rangle=2^{-1/2}[|jP\Lambda;JM\rangle+\epsilon|jP,-\Lambda;JM\rangle], \quad (9)$$

where the signed-Λ BF functions are given by[23]

$$|jP\Lambda;JM\rangle=\frac{[(2j+1)(2J+1)]^{1/2}}{4\pi}D^{J*}_{M,P}(\hat{R})D^{J*}_{P,\Lambda}(\hat{r}_b)|\Lambda\rangle, \quad (10)$$

where $\hat{r}_b\equiv(\alpha',\beta',0)$ denotes the orientation of $\hat{r}$ in the body frame.

In both the SF and BF expansions, the matrix elements of the potential matrix are usually expressed as sums of terms $V_{\lambda 0}(R)$ and $V_{\lambda,2\Lambda}(R)$, which arise in the expansion of the θ dependence of the PES's, multiplied by angular momentum coupling coefficients.[35] Specifically, $V_{\lambda 0}(R)$ and $V_{\lambda,2\Lambda}(R)$ are the expansion terms of the *sum* and *difference* of the $V_{A'}$ and $V_{A''}$ PES's, namely

$$V_{\rm sum}(R,\theta)\equiv\tfrac{1}{2}[V_{A''}(R,\theta)+V_{A'}(R,\theta)] =\sum_{\lambda=0}^{\lambda_{\max}} V_{\lambda 0}(R)d^{\lambda}_{00}(\theta) \quad (11)$$

and

$$V_{\rm dif}(R,\theta)=\frac{\eta}{2}[V_{A''}(R,\theta)-V_{A'}(R,\theta)] =\sum_{\lambda=2\Lambda}^{\lambda_{\max}} V_{\lambda,2\Lambda}(R)d^{\lambda}_{2\Lambda,0}(\theta), \quad (12)$$

where $\eta=+1$ for a Π state and -1 for a Δ state. Here $d^{\lambda}_{mn}(\theta)$ is a reduced rotation matrix element.[39] Because $d^{\lambda}_{00}(\theta)$ is equal to the regular Legendre polynomial $P_{\lambda}(\cos\theta)$,[39] Eq. (11) is identical to the more often seen Legendre expansion.

In the BF expansion, the potential matrix is block diagonal in P and independent of J.[35] Although the potential matrix is block diagonal, the centrifugal term in Eq. (4), which is diagonal in the SF expansion, has both diagonal and off-diagonal terms in the BF basis. The terms which couple different P blocks correspond to Coriolis coupling between the different BF projection states. Rather than using the basis functions defined by Eq. (9), it is more convenient to use symmetrized definite-P states, which correspond to states of well-defined parity, namely

$$|jP\epsilon\xi;JM\rangle=2^{-1/2}[|jP\epsilon;JM\rangle+\xi|j,-P\epsilon;JM\rangle], \quad (13)$$

where the additional symmetry index $\xi=\pm1$. The total parity ($\pm$) of the $|jP\epsilon\xi;JM\rangle$ functions in Eq. (13) is $\epsilon\xi(-1)^J$. For $P=0$, the basis functions are given by Eq. (9), and their total parity is $\epsilon(-1)^J$. In a more compact notation these $P=0$ basis functions will be designated 0^+ and 0^- where the sign of ϵ is given by the superscript. In the absence of Coriolis coupling, eigenfunctions of definite magnitudes of P appear in degenerate pairs for $P>0$.

By expansion of the wave function in either a BF or SF expansion, the energies and eigenfunctions of the bound states of the ArBH($A\ ^1\Pi$) complex can be obtained by determination of the $C^{JM}(R)$ expansion coefficients. This can be done either variationally or by numerical solution of the CC equations.[29] The first application to a complex of an open-shell molecule was the study by Charkravarty and Clary on ArOH,[47] who worked in a SF expansion using our earlier formulation of the Hamiltonian.[35] More qualitative insight can be obtained by examination of the adiabatic potentials which will govern the behavior of the $C^{JM}(R)$ expansion coefficients. These radial "adiabatic bender" potentials are given by

$$w_{\rm ad}(R)=T(R)W(R)T^T(R), \quad (14)$$

where $T(R)$ is the matrix which diagonalizes the $W(R)$ matrix of Eq. (4) at each value of R. The individual elements of the *vector* $w_{\rm ad}(R)$ correspond to the energies of the locally adiabatic bender (hindered rotor) states of the ArBH complex at a fixed value of the Ar–BH separation R. Hutson and co-workers[23,29] have extensively studied how these adiabatic energies depend on the relative sizes of the various $V_{\lambda}(R)$ terms in the expansion of the PES(s) [Eq. (5)]. Since the BF and SF expansion states are related by an orthogonal transformation, the locally adiabatic states are identical regardless of whether the $W(R)$ matrix is constructed in the BF or SF basis.

Since van der Waals complexes are so weakly bound, experimental studies are usually confined to supersonic nozzle preparation, so that the total angular momentum will be small. In this case, the Coriolis mixing between the various definite-P states, which varies approximately linearly with J,[29,31,45] will be small. In this case, additional physical insight can be gained by an examination of the definite-P adiabatic energies, obtained by diagonalization of the unique block of the BF $W(R)$ matrix corresponding to the chosen value of P.

These radial adiabatic bender potentials can be used to investigate the vibrational motion along the van der Waals stretching coordinate R. The energies of these vibrational levels can be obtained by solution of a one-dimensional Schrödinger equation with potential $w_{\rm ad}(R)$. To the extent that off-diagonal matrix elements of the radial kinetic energy operator can be ignored, these energies will provide a good first approximation to the bound states of the ArBH complex.

III. RADIATIVE TRANSITION STRENGTHS

In the supersonic expansions employed experimentally to prepare van der Waals complexes of diatoms, only the

This article is copyrighted as indicated in the article. Reuse of AIP content is subject to the terms at: http://scitation.aip.org/termsconditions. Downloaded to IP: 128.114.34.23 On: Mon, 01 Dec 2014 03:38:05

lowest bender-stretch level in the ground electronic state is usually expected to have significant population. For ArBH(X), we may anticipate the results of Secs. IV and V and note that the lowest ArBH(X) bender curve will have $P=0$ and correlates with the lowest [BH($X,j=0$)+Ar] rotor asymptote. The interpretation of the experiments depends crucially on the strength of the optical transitions from this bender level to the bender levels of the excited ArBH(A) complex. We expect that the dipole moment responsible for electronic transitions in the ArBH complex will be that of the BH diatom itself and will hence be perpendicular to the diatom axis for this $\Delta\Lambda=1$ transition.

Dubernet *et al.*[23] have shown that the matrix elements of the space-fixed components of the transition dipole between unsymmetrized definite-P BF basis functions [denoted as $|jP\Lambda=0;JM\rangle$ and $|j'P'\Lambda'=\pm1;J'M'\rangle$ for the ArBH(X and A) states, respectively] involves terms of the form

$$(-1)^{P'-\Lambda'}[(2j+1)(2j'+1)]^{1/2}\begin{pmatrix} J' & 1 & J \\ -P' & P' & 0 \end{pmatrix} \times\begin{pmatrix} j' & 1 & j \\ -P' & P' & 0 \end{pmatrix}\begin{pmatrix} j' & 1 & j \\ -\Lambda' & \Lambda' & 0 \end{pmatrix}. \tag{15}$$

For electric dipole transitions the selection rule on P is $\Delta P=0,\pm1$, as expressed by the first $3j$ symbol in Eq. (15). Thus, transitions are allowed from the lowest ArBH(X) bender level ($P=0$) only to excited bender levels with $P'=0$ and 1. In addition, the symmetry properties of the first $3j$ symbol[39] imply that for transitions to levels with $P'=0$ we must have $\Delta J=\pm1$, while for transitions to levels with $P'=1$ we can have $\Delta J=0,\pm1$. Finally, in the free rotor limit,[23] transitions out of the lowest ArBH(X) state, which will be well described by $j=0$, will be allowed into only the $j'=0$ and 1 ArBH(A) states. Consequently, for a weakly bound complex, in which the rotational motion of the BH moiety is not appreciably hindered, the oscillator strengths will be small for transitions from the lowest ArBH(X) bender level into ArBH(A) states with nominal values of j' greater than 1.

As discussed in Sec. II, there are two types of $P'=0$ levels, with $\epsilon'=\pm1$. We find, after some algebra, that the matrix elements of the transition dipole between definite-parity BF basis functions *vanish* for transitions from the lowest ArBH(X) bender level to the 0^- ($\epsilon=-1$) levels but are nonzero for transitions to the 0^+ ($\epsilon'=+1$) levels. Thus only *half* of the $P'=0$ levels will be observable through electric dipole transitions from the lowest ArBH(X) bender level. This selection rule will break down if there is significant Coriolis coupling; in this event, $\Delta J=0$ transitions to the "forbidden" nominal 0^- levels will acquire intensity, through mixing with $P'=1$ levels. Transitions from ArBH(X) $P=0$ to excited $P'=1$ levels will occur to one of the degenerate pair of levels for $\Delta J=\pm1$ transitions (P/R branches) and to the other level for $\Delta J=0$ transitions (Q branch).

IV. *AB INITIO* CALCULATIONS

To investigate quantitatively the energies of the ArBH complex, we carried out an *ab initio* determination of the PES for the state of A' reflection symmetry (in C_s geometry) which correlates with Ar+BH($X\,^1\Sigma^+$) and the two PES's for the states of A' and A'' reflection symmetry which correlate with Ar+BH($A\,^1\Pi$). In most of the calculations reported here, we used the recent augmented correlation-consistent valence quadruple zeta (*avqz-f*) basis of Dunning and co-workers[48,49] with the exclusion of g functions on B and Ar and the exclusion of f functions on H ($13s7p4d3f$ contracted to $6s5p4d3f$ for B, $7s4p3d$ contracted to $5s4p3d$ for H, and $17s12p4d3f$ contracted to $7s6p4d3f$ for Ar). Some exploratory calculations were carried out with the smaller augmented correlation consistent triple zeta (*avtz*) basis[48,49] ($11s6p3d2f$ contracted to $5s4p3d2f$ for B, $6s3p2d$ contracted to $4s3p2d$ for H, and $16s10p3d2f$ contracted to $6s5p3d2f$ for Ar), and with the full augmented correlation consistent quadruple zeta basis (which we denote *avqz-g*) which includes two g functions on B and Ar as well as two f functions on H. The *avtz*, *avqz-f*, and *avqz-g* bases contained of, respectively, a total of 119, 160, and 210 contracted Gaussian functions. All calculations were carried out with the MOLPRO suite of *ab initio* programs.[50] In all the calculations reported here, the BH bond distance was held to $r=1.2324$ and $r=1.2186$ Å, the experimental equilibrium bond lengths in the BH $X\,^1\Sigma^+$ and $A\,^1\Pi$ states, respectively.[51]

The interaction energy for each state can be defined as

$$V(R,\theta)=E_{\text{Ar-BH}}(R,\theta)-E_{\text{BH}}(\infty)-E_{\text{Ar}}(\infty) -\Delta E_{\text{CP}}(R,\theta)-\Delta E_{\text{SC}}(R,\theta). \tag{16}$$

Here the counterpoise correction, which adjusts for the lack of saturation of the orbital basis is defined by[52]

$$\Delta E_{\text{CP}}=E_{\text{BH}}(R,\theta)+E_{\text{Ar}}(R,\theta)-E_{\text{BH}}(\infty)-E_{\text{Ar}}(\infty) \tag{17a}$$

and the residual size consistency of the calculations is defined by

$$\Delta E_{\text{SC}}=E_{\text{Ar-BH}}(\infty)-E_{\text{BH}}(\infty)-E_{\text{Ar}}(\infty). \tag{17b}$$

In the determination of the geometry dependence of the PES's we performed complete-active-space SCF (CASSCF) (Refs. 53 and 54) calculations followed by multireference, internally contracted (Refs. 55 and 56) configuration interaction (MRCI) calculations. In these calculations the active space in the CASSCF calculations was constructed by distributing the *four* outer BH electrons (all electrons exclusive of the B $1s$) among the *five* outer BH orbitals ($2\sigma,3\sigma,4\sigma,1\pi_x,1\pi_y$). The CASSCF orbitals were obtained by a state-averaging procedure[57–59] in which equal weights were assigned to the following three BH states: $X\,^1\Sigma^+$, $A\,^1\Pi_x$, and $A\,^1\Pi_y$. In C_s geometry the reference space for the subsequent internally contracted CI calculations consisted of 1316 *csf*'s for the states of $^1A'$ symmetry, and 1204 *csf*'s for the states of $^1A''$ symmetry. The CI calculations included all single and double excitations out of this reference space with the exclusion of excitations out of the lower five orbitals of a', and the lowest orbital of a'', sym-

This article is copyrighted as indicated in the article. Reuse of AIP content is subject to the terms at: http://scitation.aip.org/termsconditions. Downloaded to IP: 128.114.34.22 On: Mon, 01 Dec 2014 02:24:03

TABLE I. Comparison of the calculated ArBH(X) potential energy surface for perpendicular approach of the Ar atom (energies in cm^{-1}; distances in bohr).

	avtz[a]				*avqz-f*[b]
R (bohr)	MR-CI	CEPA	MR-ACPF	MR-CI(D)	MR-CI(D)
12.0	−4.77	−5.61	−5.88	−5.86	−6.06
11.0	−8.33	−9.69	−10.23	−10.21	−10.52
10.0	−15.23	−17.52	−18.61	−18.59	−19.13
9.0	−28.61	−32.55	−34.81	−34.87	−35.86
8.0	−51.05	−58.33	−63.22	−63.62	−65.72
7.5	−62.50	−72.93	−80.25	−81.00	−84.38
7.0	−64.29	−79.86	−91.00	−92.28	−97.97
6.5	−33.10	−57.31	−74.53	−76.58	−86.39
6.0	86.55	47.67	20.46	17.33	0.18
5.5	415.59	351.16	307.71	303.21	273.67
5.0	1196.79	1086.39	1018.02	1012.15	964.20
4.5	2885.20	2698.62	2587.85	2581.84	2507.50

[a]Augmented valence correlation-consistent triplet-zeta basis (Refs. 48 and 49).
[b]Augmented valence correlation-consistent quadruple-zeta basis (Refs. 48 and 49) *without g* functions on B and Ar and without *f* functions on H.

metry (which correspond to the B $1s$ orbital and the $n=1$ and $n=2$ shells of Ar). The contribution of higher-order excitations was then estimated using the internally contracted multireference version[60] of the Davidson correction [MR-CI(D)].[61]

As a calibration of the *avqz* basis set, Tables I and II compare, respectively, the calculated ArBH(X) and ArBH(A) energies for perpendicular ($\theta=90°$) approach of the Ar atom. Table I also compares the MR-CI and MR-CI(D) energies with those determined with the internally contracted multireference version[60] of the coupled pair functional method of Gadnitz and Ahlrichs (MR-ACPF) (Refs. 62) and the correlated electron pair method of Meyer (Refs. 2,3, and 63). The MR-CI(D) and MR-ACPF calculations with the same basis set are seen to give virtually identical results. The MR-CI interaction potentials are less attractive, as would be anticipated, because of the lack of inclusion of higher-order excitations. The CEPA results are intermediate. Both for the ArBH(X) PES (Table I) and the ArBH(A) PES's (Table II), a slightly more attractive well is predicted by the calculations with the larger (*avqz-f*) basis set. To estimate the contribution of g functions, we carried out some additional calculations, with the full *avqz-g* basis. To minimize computational effort, and the size of the integral files, these additional calculations were done for colinear geometry. The calculated energies are tabulated in Table III.

The major limitation in the present *ab initio* calculations is our inability to account precisely for the effect of higher order excitations. This drawback is particularly severe because we were unable to include in the active space any virtual excitations of the Ar electrons. Unfortunately, the virtual Ar orbitals lie considerably higher than many of the BH Rydberg orbitals. Thus, inclusion into the reference space of

TABLE II. Comparison of ArBH(A) MR-CI(D) potential energy surfaces for perpendicular approach of the Ar atom (energies in cm^{-1}; distances in bohr).

	$V_{A'}$		$V_{A''}$	
R (bohr)	*avtz*[a]	*avqz-f*[b]	*avtz*[a]	*avqz-f*[b]
10.0	−25.73	−27.70	−20.30	−20.88
8.0	−23.92	−31.35	−75.91	−78.06
7.0	130.30	116.61	−136.74	−142.71
6.0	916.40	888.01	−156.13	−174.60
5.5	2017.49	1973.49	−40.08	−72.27
5.0	4217.25	4148.06	337.74	285.29

[a]Augmented valence correlation-consistent triplet-zeta basis (Refs. 48 and 49).
[b]Augmented valence correlation-consistent quadruple-zeta basis (Refs. 48 and 49) *without g* functions on B and Ar and without *f* functions on H.

TABLE III. Comparison of ArBH MR-CI(D) potential energy surfaces for colinear approach of the Ar atom. Energies in cm^{-1}, distances in bohr. Energies from multireference configuration-interaction calculation with Davidson correction.

	ArBH($X\ ^1\Sigma^+$)		ArBH($A\ ^1\Pi$)	
R (bohr)	*avqz-f*[a]	*avqz-g*[b]	*avqz-f*[a]	*avqz-g*[b]
		Ar–HB		
11.0	−16.24	−16.11	−16.45	−16.34
10.0	−29.56	−29.50	−30.97	−30.87
9.0	−47.18	−47.74	−57.75	−57.98
8.0	−17.24	−21.60	−82.73	−85.47
7.5	99.30	89.05	−54.10	−60.94
7.0	438.19	416.71	89.86	75.02
6.5	1313.48	1273.45	542.20	513.99
		Ar–BH		
11.0	−16.81	−16.75	−14.25	−14.18
10.0	−30.28	−30.29	−25.70	−25.64
9.0	−50.90	−51.42	−44.60	−44.88
8.5	−59.59	−60.86	−54.91	−55.85
8.0	−55.88	−59.06	−59.77	−62.07
7.5	−15.56	−22.35	−45.10	−50.32
7.0	117.71	104.40	20.36	9.88
6.5	467.30	443.48	202.00	183.60

[a]Augmented valence correlation-consistent quadruple-zeta basis (Refs. 48 and 49) *without g* functions on B and Ar and without *f* functions on H.
[b]Augmented valence correlation-consistent quadruple-zeta basis (Refs. 48 and 49).

This article is copyrighted as indicated in the article. Reuse of AIP content is subject to the terms at: http://scitation.aip.org/termsconditions. Downloaded to IP:

TABLE IV. Comparison of MR-CI, MR-CI(D), CEPA, CCSD(T), and QCI ArBH(X) potential energy surfaces. Energies in cm^{-1}, distances in bohr, augmented valence correlation-consistent quadruple-zeta basis (Refs. 48 and 49) *without* g functions on B and Ar and without f functions on H.

R (bohr)	MR-CI	MR-CI(D)	CEPA	CCSD(T)	QCI
		θ=0° (Ar–HB)			
11.0	−12.57	−16.24	−15.62	−14.99	−14.99
10.0	−22.64	−29.56	−28.24	−27.13	−27.00
9.0	−32.54	−47.18	−43.99	−41.72	−41.42
8.0	15.01	−17.24	−8.66	−4.64	−3.90
7.5	147.57	99.30	113.92	118.54	119.63
7.0	510.92	438.19	462.93	467.60	469.17
6.5	1424.50	1313.48	1352.93	1358.50	1360.64
		θ=90° (T shaped)			
11.0	−8.81	−10.52	−9.70	−9.64	−9.60
10.0	−15.89	−19.13	−17.53	−17.49	−17.43
9.0	−29.51	−35.86	−32.56	−32.50	−32.49
8.0	−52.66	−65.73	−58.34	−58.35	−58.33
7.5	−65.11	−84.38	−72.94	−73.01	−73.00
7.0	−68.83	−97.98	−79.87	−80.05	−80.03
6.5	−41.14	−86.39	−57.32	−57.64	−57.62
6.0	72.17	0.18			
		θ=180° (Ar–BH)			
11.0	−13.81	−16.81	−15.77	−15.01	−14.96
10.0	−24.56	−30.28	−28.18	−26.65	−26.43
9.0	−39.23	−50.90	−46.42	−43.00	−42.45
8.0	−30.86	−55.88	−45.69	−37.39	−36.14
7.5	21.52	−15.56	0.12	13.34	15.13
7.0	173.09	117.71	142.14	163.29	165.83
6.5	550.65	467.30	505.69	540.01	543.47

excitations of the Ar $3p$ electrons into higher Ar orbitals of s, p, and d symmetry, would so expand the active space as to render the calculations prohibitively time consuming. As an additional estimate of the effect of higher order excitations, we carried out, also with the $avqz$-f basis, coupled cluster (singles and doubles) calculations[64] with perturbative inclusion of the triple excitations[65] for the ArBH(X) PES. These CCSD(T) calculations are possible for the closed-shell ArBH(X) state, but not for ArBH(A) where the electron occupancy corresponds to two singly filled orbitals. Table IV compares the counterpoise corrected CCSD(T), and related quadratic CI (QCI) interaction energies, with the previously determined MR-CI(D) values and those from the correlated electron pair method. We observe that the CCSD(T) and QCI interaction energies are virtually identical, and both are quite similar to the CEPA interaction energies. The depth of the attractive well is slightly less than predicted by the CEPA calculations, and substantially less than predicted by the MR-CI(D) calculations.

MR-CI calculations of the ArBH(X) and ArBH(A) potential energy surfaces were carried out at seven values of θ (0°, 30°, 60°, 90°, 120°, 150°, and 180°) and eleven values of the center-of-mass separation R (4.5, 5, 5.5, 6, 6.5, 7, 8, 9, 10, 11, and 12 bohr). For each value of θ the PES's were fit as a function of R to the general functional form[66]

$$V(R,\theta_i)=c_1\exp(-b_1R)+(c_2+c_3R)\exp(-b_2R) + c_4\{\tanh[1.2(R-R_0)]+1\}/R^6, \quad (18)$$

The root mean square relative error in the fit was <0.1%. In the determination of the angular expansion coefficients in Eq. (11) we took λ_{max} equal to 6, the upper limit imposed by the number of different values of θ at which *ab initio* calculations were carried out.

Figures 1 and 2 present contour plots of the PES's for the ArBH(X,A) electronic states. Table V lists the geometries of the minima and the dissociation energies. The equilibrium geometry of the ArBH(X) state is approximately T shaped. Further, it is obvious from Fig. 1 that the ArBH(X) repulsive wall is quite anisotropic. The ArBH(A) PES's of A' and A'' symmetry are quite different, reflecting the increased Pauli repulsion when the electron in the singly filled 1π orbital is in the triatomic plane. The A'' PES is significantly more attractive, with an approximately T-shaped equilibrium geometry. The A' PES possesses two shallower minima. Figure 3 displays the radial dependence of the angular expansion coefficients $V_{\lambda 0}(R)$ and $V_{\lambda 2}(R)$. Consistent with the large difference in the ArBH(A) PES's of A' and A'' symmetry, the largest *anisotropic* $V_{\lambda\mu}(R)$ term, exclusive of the *isotropic* $V_{00}(R)$ term, is the first term in the angular expansion of V_{dif}, namely $V_{22}(R)$.

As a result of our inability to include higher order excitations involving the Ar electrons, we anticipate that the true BH–Ar van der Waals well depths will be ~50–100 cm^{-1} deeper and the position of the minimum ~0.2–0.4 bohr closer in than predicted by our calculations. This conclusion is based both on a comparison between our calculations on the BAr($X\,^2\Pi$,$B\,^2\Sigma^+$) potential energy curves and the experimentally derived information on these electronic states,[67]

This article is copyrighted as indicated in the article. Reuse of AIP content is subject to the terms at: http://scitation.aip.org/termsconditions. Downloaded to IP: 128.114.34.22 On: Mon, 01 Dec 2014 02:28:05

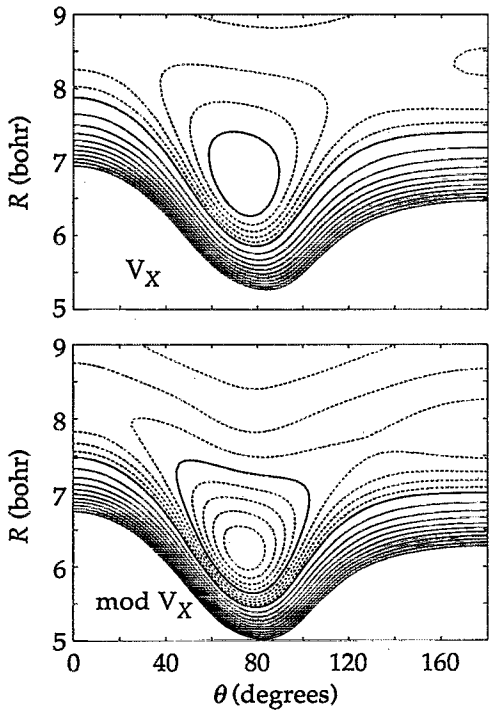

FIG. 1. Contour plot of the ArBH(X) PES (upper panel) and modified ArBH(X) PES (lower panel). The linear BHAr geometry corresponds to θ=0°. The dashed contours indicate negative energies with the first contour at -20 cm^{-1}, a spacing of 20 cm^{-1}, and the last contour at -100 cm^{-1} (upper panel) and -180 cm^{-1} (lower panel). The solid contours designate positive energies; the contours are equally spaced with the first contour at 50 cm^{-1}, a spacing of 50 cm^{-1}, and the last (innermost) contour at 500 cm^{-1}. For clarity, the contours at 0 and -100 cm^{-1} are drawn with heavy solid curves.

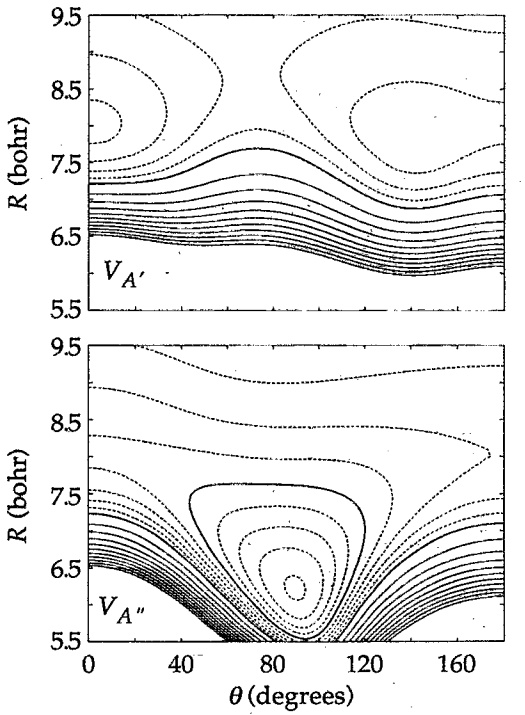

FIG. 2. Contour plots of the ArBH(A) PES's for the states of A' (upper panel) and A'' (lower panel) reflection symmetry. The linear BHAr geometry corresponds to θ=0°. The dashed contours indicate negative energies with the first contour at -10 cm^{-1} and a spacing of 10 cm^{-1}. The solid contours designate positive energies; the contours are equally spaced with the first contour at 50 cm^{-1}, a spacing of 50 cm^{-1}, and the last (innermost) contour at 500 cm^{-1}. For clarity, the contours at 0 and -100 cm^{-1} are drawn with heavy solid curves.

and a similar comparison between single-reference CI-SD and CEPA calculations of the Ar_2 dimer and the experimentally derived[68] potential for this dimer. The comparison for Ar_2 is shown in Fig. 4.

In order to simulate this expected deepening and contraction of the PES's, without changing the qualitative form of the PES's, we constructed a set of modified PES's by modifying each calculated $V(R,\theta_i)$ potential curve as

$$V_{\text{mod}}(R,\theta_i)=V(R+0.4,\theta_i)(1+\tfrac{1}{3}\{\tanh[1.2(R-R_{ei}+0.5)]+1\}), \quad (19)$$

where R_{ei} is the position of the minimum of $V(R,\theta_i)$. At long range the transformation described by Eq. (19) increases the attractive tail of the potential by a factor of 5/3.

At short range the potential is translated inward by 0.4 bohr but is otherwise unchanged. As can be seen in Fig. 4, this entirely *ad hoc* modification brings the calculated Ar_2 potential curve in far closer agreement with the experimentally derived[68] potential for this dimer, at least in the region of the van der Waals well. In addition, and as will be discussed further in the following article,[21] the *ab initio* PES's predict zero-point corrected dissociation energies for both ArBH(X) and ArBH(A) which are too small by roughly 40% and, further, predict rotational constants for these complexes which are also too small, indicative of too large an Ar–BH separation. However, with the *ad hoc* modification of Eq. (19), excellent agreement is obtained for both the dissociation energies and the rotational constants.

Contour plots of the modified ArBH PES's are shown in the lower panel of Figs. 1 [ArBH(X)] and 5 [ArBH(A)], and the equilibrium geometry and dissociation energies are listed in Table V. As can be seen in the comparison with the upper panel of Figs. 1 and 2, the modified PES's are deeper and shifted inward, but otherwise qualitatively unchanged. The angular expansion coefficients $V_{\lambda 0}(R)$ and $V_{\lambda 2}(R)$ for the modified PES's are displayed in Fig. 6.

TABLE V. Equilibrium geometries and dissociation energies of ArBH complexes.

State	θ_e	R_e (bohr)	D_e (cm^{-1})
		Ab initio PES's	
ArBH(X)	74.0	6.70	125
ArBH(A)$V_{A'}$[a]	0.0	8.02	85
	125.0	7.98	69
ArBH(A)$V_{A''}$	89.5	6.22	183
		Modified PES's	
ArBH(X)	74.5	6.22	198
ArBH(A)$V_{A'}$[a]	0.0	7.76	128
	139.0	7.64	112
ArBH(A)$V_{A''}$	88.5	5.97	280

[a]There are two minima on the A' ArBH(A) PES's; see Figs. 2 and 5.

This article is copyrighted as indicated in the article. Reuse of AIP content is subject to the terms at: http://scitation.aip.org/termsconditions. Downloaded to IP: 128.114.34.22 On: Mon, 01 Dec 2014 02:28:05

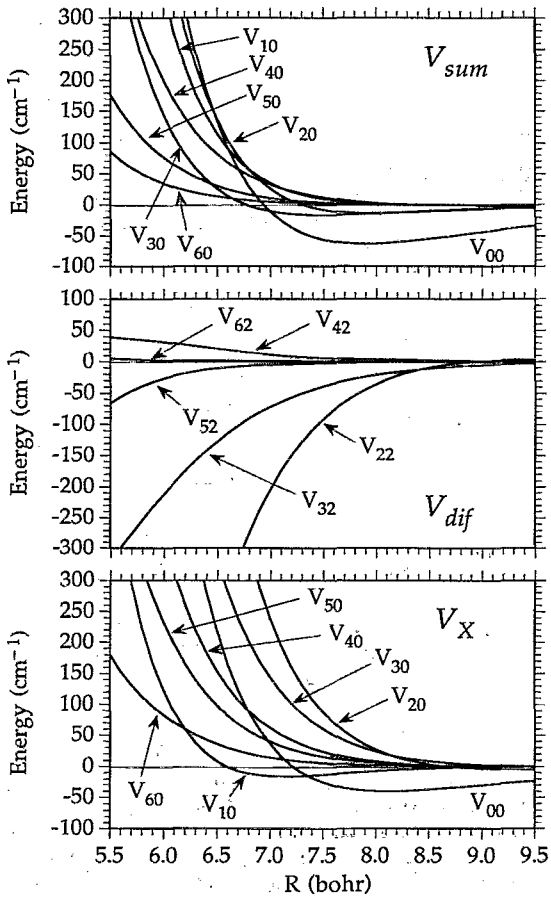

FIG. 3. Plots of the coefficients in the expansion in reduced rotation matrix elements of the MR-CI(D) ArBH(A) and ArBH(X) PES's. (Upper panel) Coefficients $V_{\lambda 0}(R)$ in the expansion of the average ArBH(A) potential [Eq. (11)]; (middle panel) coefficients $V_{\lambda 2}(R)$ in the expansion of the difference ArBH(A) potential [Eq. (12)]; (lower panel) coefficients $V_{\lambda}(R)$ in the expansion of the nondegenerate ArBH(X) potential.

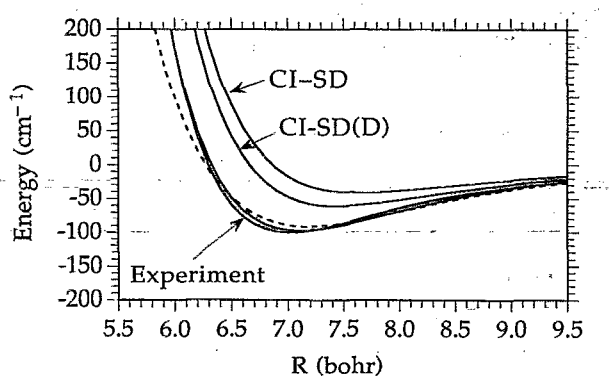

FIG. 4. Comparison of the experimentally derived potential curves for the Ar_2 dimer (curves MSV-II and MSV-III from Ref. 68) with CI-SD and CI-SD(D) curves calculated with the *avqz-f* basis set. The dashed curve is the CI-SD(D) curve modified according to the prescription given by Eq. (19).

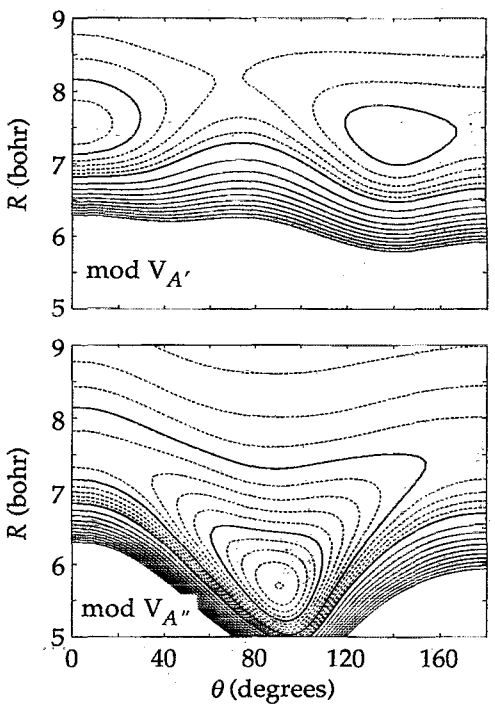

FIG. 5. Contour plots of the ArBH(A) PES's for the states of A' (upper panel) and A'' (lower panel) reflection symmetry, modified as described by Eq. (19). The linear BHAr geometry corresponds to θ=0°. The dashed contours indicate negative energies with the first contour at -10 cm^{-1} and a spacing of 10 cm^{-1}. The solid contours designate positive energies; the contours are equally spaced with the first contour at 50 cm^{-1}, a spacing of 50 cm^{-1}, and the last (innermost) contour at 500 cm^{-1}. For clarity, the contours at 0, -100, and -200 cm^{-1} are drawn with heavy solid curves. In comparing this figure with Fig. 2, which presents the *unmodified* ArBH(A) PES's, the reader should note that the ordinates in Fig. 5 have been shifted in by 0.5 bohr relative to those in Fig. 2.

V. CALCULATED BEND-STRETCH ENERGIES OF THE ArBH COMPLEX

A. Adiabatic bender potentials

Adiabatic radial potentials for various bender states for ArBH in both the $X\ ^1\Sigma^+$ and $A\ ^1\Pi$ electronic states were calculated by solution of the CC equations in the SF basis. In addition, similar calculations of the definite-P adiabatic radial potentials were carried out within the centrifugal decoupling (CD, also called "coupled-states") approximation.[69] In the CD approximation, the BF equations in the absence of Coriolis coupling are additionally modified by replacement of the true diagonal centrifugal barrier[31,45]

$$\hbar^2[J(J+1)+j(j+1)-2P^2]/2\mu R^2 \qquad (20)$$

by the diagonal matrix

$$\hbar^2\bar{l}(\bar{l}+1)/2\mu R^2, \qquad (21)$$

where $\bar{l}$ is an effective angular momentum, taken to be the same for all channels. For the calculation of the asymptotic diatom rotational energies, the BH rotational constants and the $A\ ^1\Pi$ Λ doubling splitting parameter were taken from the spectroscopic study of Fernando and Bernath.[70] All calculations of the adiabatic potentials, for various values of the

This article is copyrighted as indicated in the article. Reuse of AIP content is subject to the terms at: http://scitation.aip.org/termsconditions. Downloaded to IP: 128.114.34.22 On: Mon, 01 Dec 2014 02:28:05

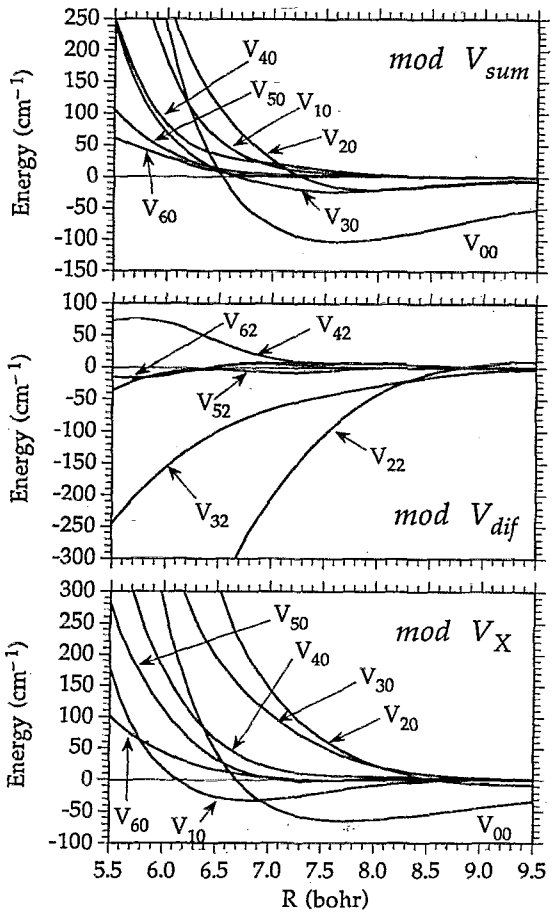

FIG. 6. Plots of the coefficients in the expansion in reduced rotation matrix elements of the MR-CI(D) ArBH(A) and ArBH(X) PES's, modified as described by Eq. (19). (Upper panel) Coefficients $V_{\lambda 0}(R)$ in the expansion of the average ArBH(A) potential [Eq. (11)]; (middle panel) coefficients $V_{\lambda 2}(R)$ in the expansion of the difference ArBH(A) potential [Eq. (12)]; (lower panel) coefficients $V_{\lambda}(R)$ in the expansion of the nondegenerate ArBH(X) potential.

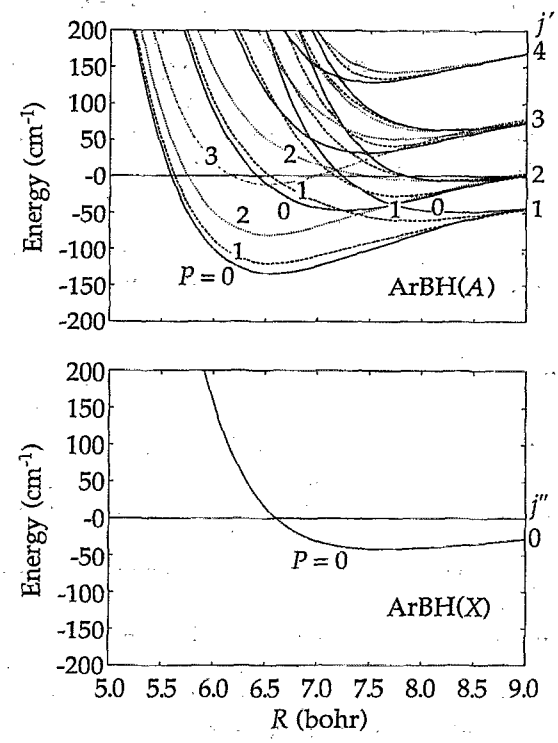

FIG. 7. Radial adiabatic bender potential energy curves for the ArBH system within the centrifugal decoupling approximation for an effective total angular momentum $\bar{l}=1$, and determined using the unmodified MR-CI(D) PES's. The upper panel displays the adiabatic bender potentials for ArBH(A). The correspondence of the asymptotes with the rotational levels of the BH($A\ ^1\Pi$) fragment is indicated. Also shown are the P labels associated with the lower curves. In addition there will be two $P=3$ curves correlating with both $j=3$ and 4, and two $P=4$ curves correlating with $j=4$. For clarity, the $P=3$ and $P=4$ curves are not shown, except (dotted-dash line) for the strongly bound $P=3$ curve which correlates with $j=3$. Note that in a full close-coupled treatment the lower of the two $P=0$ levels correlating with BH($j=1$) exists only for negative parity, and the upper, only for positive parity. The lower panel displays the lowest adiabatic bender potential for ArBH(X).

total angular momentum J, as well as the exact vibrational energies presented in Sec. V B, were carried out with our Hibridon code.[71]

In interpreting the adiabatic curves, it is instructive to consider how the various terms in the interaction potentials influence the number and ordering of bender states. Dubernet *et al.*[23] have considered this general question for various classes of open-shell van der Waals complexes. In this work they assumed that the difference potential $V_{\rm dif}$ would be small, as it is in ArOH($X\ ^2\Pi$).[4] Here, however, we see from Figs. 3 and 6 that for ArBH($A\ ^1\Pi$) the leading term in the angular expansion of the difference potential (V_{22}) is comparable in magnitude to the leading term in the expansion of the sum potential (V_{20}). Consequently, we must consider explicitly the effect of $V_{\rm dif}$ on the various bender states. For the lowest rotor asymptote ($j=1$) of a $^1\Pi$ diatom electronic state, approach of a spherical partner gives rise to 6 different bender states, because of the rotational $(2j+1)$ and electronic orbital ($\Lambda=\pm 1$) degeneracy. Using the magnitude of P and the total parity as labels, these correspond to two $P=0$ levels, of + and − total parity, and four $P=1$ levels, in two pairs of ± parity. As in the analysis of Dubernet *et al.*,[23] in the simplest approximation we retain only three anisotropic terms, in this case V_{10}, V_{20}, and V_{22}. As discussed by Dubernet *et al.*[23] if solely the V_{20} term is nonzero (as for a homonuclear diatom), the six degenerate levels will split into two sets, corresponding to $P=0$ (two levels) and $P=1$ (four levels). The degeneracy of the latter will be raised by the presence of a nonzero V_{10} term, which will give rise to three sets of levels: a degenerate pair of $P=0$ levels and two degenerate pairs of $P=1$ levels. If, in addition, we allow V_{22} to be nonzero, the energies of the two $P=0$ levels [which we can denote as 0^+ and 0^-—see the discussion after Eq. (13)] will become distinct. This splitting of the $P=0$ levels is formally equivalent to the splitting of diatomic molecule Hund's case (a) $^3\Pi_{0^+}$ and $^3\Pi_{0^-}$ levels, or case (c) $\Omega=0^+$ and 0^- levels, whose energies are slightly different even in the absence of molecular rotation.[41,72]

Figure 7 presents adiabatic CD bender potential energy curves for ArBH(A) for a total angular momentum $J=1$. Also shown is the lowest adiabatic bender potential for ArBH(X), which corresponds to $P=0$. The splitting be-

This article is copyrighted as indicated in the article. Reuse of AIP content is subject to the terms at: http://scitation.aip.org/termsconditions. Downloaded to IP:

tween the two ArBH(A) $P=0$ adiabatic bender potential curves is large. In a full CC treatment, the lowest $P=0$ curve which correlates with the $j=1$ rotor asymptote is found to have + total parity and hence $\epsilon=-1$, while the upper $P=0$ curve which correlates with the same asymptote has $-$parity, and hence $\epsilon=+1$. There are avoided crossings between the various bender curves, but the effect of these crossings is very localized.

At the low J's sampled in the experiment of Hwang and Dagdigian,[21] the Coriolis coupling is so small compared with the energy differences between the bender curves that P is a nearly good quantum number for this system; the corresponding CC adiabatic bender potential curves are virtually identical to those shown in Fig. 7. Since the 0^+ and 0^- levels are already split strongly by the V_{22} term, the very small Coriolis coupling of these levels to levels with $P=\pm 1$ will have a negligible effect on the positions of the levels, unless either of these states accidentally happens to be degenerate with a $P=1$ state. (There is no Coriolis coupling between 0^+ and 0^- states.)

However, Coriolis coupling will lift the degeneracy of the $P>0$ levels, which will split in a J-dependent fashion. As in the Λ doubling of a $^1\Pi$ diatomic electronic state[41,72] and the l-type doubling in degenerate bending vibrational levels of a triatomic molecule,[73] the splitting of the $P=1$ levels will be proportional to $J(J+1)$ if the perturbing $P=0$ levels lie not too nearby. The effect of Coriolis coupling, and, in particular, this splitting, is illustrated by Table VI, which lists, for $J=1$, 5, and 9, this parity splitting of the lowest three $P=1$ adiabatic bender states, evaluated near the minima of the respective potential curves. This splitting, which does scale well with $J(J+1)$, is seen to be microscopically small for the lowest $P=1$ state, which is well separated from other states, but somewhat larger, although still small, for the higher $P=1$ states, which lie near perturbing $P=0$ and 2 levels.

Apparent in the upper panel of Fig. 7 is a set of strongly bound bender curves with $P=0$, 1, 2, and 3, which correlate, respectively, with $j=1$, 1, 2, and 3, respectively, and which all have their minima at $R\approx 6.5$ bohr. The energies at their respective minima (including the corresponding $P=4$ curve, which correlates with $j=4$ and which is not shown in Fig. 7) are well fit by the formula for a rigid symmetric top with $A=12.42$ cm^{-1}, so that the successively higher curves correspond to states of higher internal BH rotational motion. This value of A is close to what one would calculate for a rigid ArBH complex with $R=6.5$ bohr and $\theta=90°$, approximately the equilibrium geometry of the ArBH(A) PES of A'' symmetry (see Table V). It is thus tempting to assume that these bender curves represent motion on this PES alone. By setting V_{dif} equal to zero and taking V_{sum} equal to either $V_{A'}$ or $V_{A''}$, we can determine the adiabatic bender potentials appropriate to motion on the A'' or A' PES's separately. These are shown in Fig. 8 and compared to the lower adiabatic bender curves for the full potential (both $V_{A'}$ and $V_{A''}$ PES's.

TABLE VI. Splitting (in cm^{-1}) between $P=1$ ArBH(A) adiabatic bender levels at potential minima as a function of J.

		$\Delta E(P=1, n)$[a]		
n	R	$J=1$	$J=5$	$J=9$
1	6.575	<−0.01	−0.04	−0.10
2	7.925	0.005	0.066	0.198
3	7.775	0.077	0.379	1.071

[a]Difference in energy between nth $P=1$ adiabatic bender curves of positive and negative parities, evaluated close to the minima in the respective potential curves. The $n=1$, 2, and 3 adiabatic bender curves are labeled in Fig. 7.

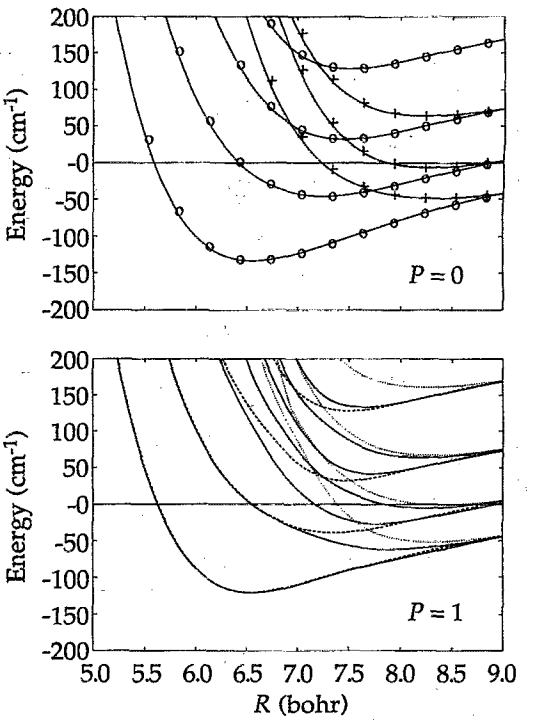

FIG. 8. (Upper panel) Comparison of the CD radial adiabatic bender potential energy curves for $P=0$ for ArBH(A) (solid curves) with comparable adiabatic bender curves for motion solely on the $V_{A'}$ (+'s) or on the $V_{A''}$ (o's) PES. (Lower panel) Similar comparison but for $P=1$. Here the dashed lines designate the adiabatic bender curves for motion solely on the $V_{A'}$ PES and the dotted lines, for motion solely on the $V_{A''}$ PES.

We observe in Fig. 8 that the $P=0$ adiabatic bender potentials lie virtually on top of those corresponding to motion on the separate PES's. The short range behavior of the $P=1$ adiabatic bender curves are identical to those characteristic of motion on the $V_{A''}$ PES. At larger distances, however, there is clearly considerable mixing between the $V_{A'}$ and $V_{A''}$ PES's. Thus we conclude, as anticipated in the preceding paragraph, that the strongly bound set of bender potentials with $P=0$, 1, 2, 3,..., which all have their minima at $R\approx 6.5$ bohr, correspond to ArBH(A) states whose vibrational motion is governed primarily by the $V_{A''}$ PES. For $j>1$, there is one of these strongly bound curves which correlate with each successive j asymptote (see Fig. 7), and the projection quantum number associated with each curve corresponds to $P=j$. The states which are described by these curves correspond to helicopterlike motion of the BH(A) with respect to R, in which, in the large-j limit, the internal

This article is copyrighted as indicated in the article. Reuse of AIP content is subject to the terms at: http://scitation.aip.org/termsconditions. Downloaded to IP: 128.114.34.22 On: Mon, 01 Dec 2014 02:28:03

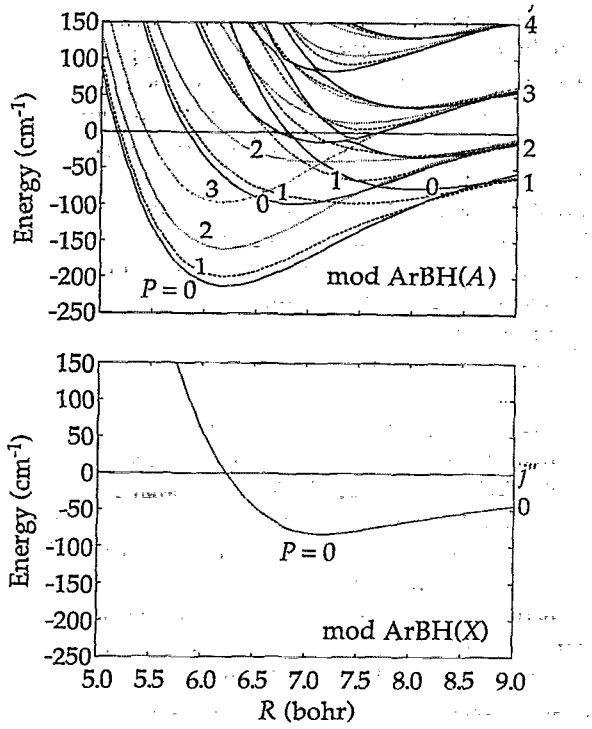

FIG. 9. Radial adiabatic bender potential energy curves for the ArBH system within the centrifugal decoupling approximation for an effective total angular momentum $\bar{l}=1$, and determined using the MR-CI(D) PES's, modified as described at the end of Sec. IV. The upper panel displays the adiabatic bender potentials for ArBH(A). The correspondence of the asymptotes with the rotational levels of the BH($A\ ^1\Pi$) fragment is indicated. Also shown are the P labels associated with the lower curves. In addition there will be two $P=3$ curves correlating with both $j=3$ and 4, and two $P=4$ curves correlating with $j=4$. For clarity, the $P=3$ and $P=4$ curves are not shown, except (dotted-dash line) for the strongly bound $P=3$ curve which correlates with $j=3$. Note that in a full close-coupled treatment the lower of the two $P=0$ levels correlating with BH($j=1$) exists only for negative parity, and the upper, only for positive parity. The lower panel displays the lowest adiabatic bender potential for ArBH(X).

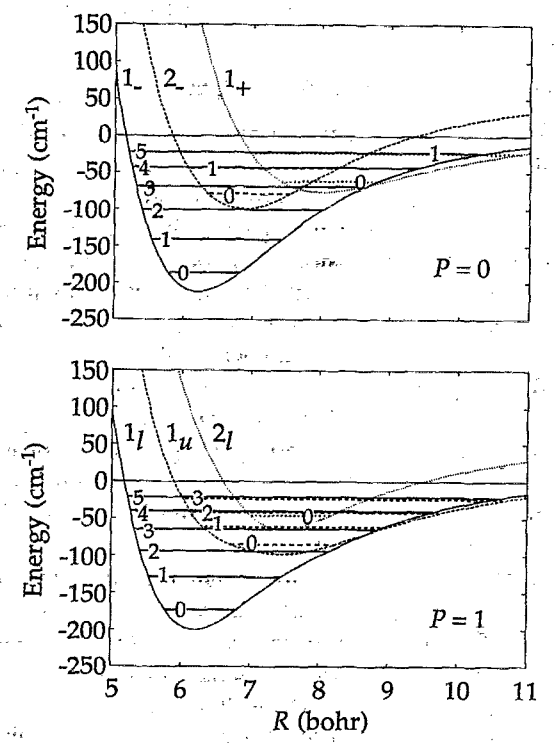

FIG. 10. Positions of the lower ArBH(A) van der Waals stretch levels (and vibrational assignments) determined from the $P=0$ and 1 radial adiabatic bender potential energy curves shown in Fig. 9. In the upper panel, the solid, dashed, and dotted lines correspond, respectively, to the 1_-, 2_-, and 1_+ levels (see Table VII). In the lower panel, the solid, dashed, and dotted lines correspond, respectively, to the 1_l, 1_u, and 2_l levels (see Table VII).

rotation of the BH moiety is confined to a plane perpendicular to $\bar{R}$.

In addition to the strongly bound bender curves discussed earlier, there are numerous, more weakly bound bender curves with larger Ar–BH separations at their minima ($R_e \approx 7.5-8$ bohr). There are also numerous avoided crossings of these bender curves. Further, the lower panel of Fig. 8 indicates these curves correspond to correlated motion on both the $V_{A'}$ and $V_{A''}$ PES's.

Figure 9 displays CD adiabatic bender potentials derived from the modified ArBH(X,A) PES's. These curves are qualitatively *identical* to the adiabatic bender potentials derived from the *ab initio* ArBH(X,A) PES's, which are shown in Fig. 7, but deepened a bit and shifted slightly toward shorter internuclear distance.

Within the adiabatic bender approximation, estimates of the stretch-bend energies of the complex can be obtained by numerical integration of the one-dimensional CD adiabatic bender potentials shown in Figs. 7 and 9. Because the avoided crossings shown in Figs. 7 and 9 are highly localized, the calculated adiabatic bender curves were first uncrossed (diabatized). For the modified PES's, the calculated adiabatic bender stretch-bend energies are listed in Table VII. Also noted in this table are the projection quantum number P and the rotational level j of the BH molecule to which the particular adiabatic bender potential correlates asymptotically. Since for each P there are *two* adiabatic bender potentials which correlate with each rotational level of the BH molecule, we add an additional subscript to this BH rotational index. As discussed in Sec. II, the two $P=0$ bender levels differ in their total parity. In Table VII we designate the parity for $P=0$ levels by a subscript ($\pm$) on the asymptotic rotational quantum number according to the sign of the symmetry index $\epsilon=\pm 1$. In the case of $P>0$ states, the subscripts u and l will designate the upper (higher energy) or lower (lower energy) of the adiabatic bender curves which correlate with each value of j. Finally, we also label the energy levels in Table VII with the vibrational quantum number v_s of the Ar–BH van der Waals stretch motion. Because the adiabatic bender energies will be seen to be an excellent approximation to the full CC energies (see Sec. V B), we advocate the use of this labeling scheme in assigning the observed levels of the ArBH complex, rather than other labeling schemes borrowed from those used for more rigid triatomics.[20,22,74]

The positions of the lower bend stretch levels for $P=0$ and 1 are illustrated pictorially in Fig. 10. It can be seen that the pattern of ArBH(A) vibrational levels is complex be-

This article is copyrighted as indicated in the article. Reuse of AIP content is subject to the terms at: http://scitation.aip.org/termsconditions. Downloaded to IP:

cause of the interleaving of stretch levels supported by different bender curves.

B. Exact ArBH vibrational energies

Finally, we present the results of exact calculations of the vibrational levels of the ArBH van der Waals complex, using the CC expansion of Eqs. (1) and (7), and the CD approximation. For the latter calculations and for CC calculations at the lowest possible value of the total angular momentum ($J=1$), a distributed Gaussian basis[75] is used for the radial expansion coefficients in Eq. (1). A total of 46 functions with an exponential parameter[75] A of 0.3 were used, spaced equally over the range $4 \leqslant R \leqslant 18$ bohr. The required matrix elements in this Gaussian basis were obtained by numerical integration using a 560 point grid. Convergence of the calculated ArBH bend-stretch energies to within less than 0.02 cm^{-1} could be obtained by retaining rotational states with $j \leqslant 7$ in the expansion.

At higher values of the total angular momentum, due to the $2j+1$ projection degeneracy of each rotational level, the dimensionality of the combined rotational-distributed Gaussian basis becomes prohibitively large. In particular, at $J=5$, there are 57 rotational states with $j \leqslant 7$. This results in a primitive basis of dimensionality $n=2622$. As an alternative, for $J>1$ (specifically, $J=5$) we use instead a contracted basis in R built out of the lower states from a CD calculation in the primitive (distributed Gaussian basis). Specifically, for each value of j retained in the rotational basis we carried out CD calculations limited to just this one value of j. We then kept the vibrational wave functions for the lowest ten CD states with $P=0$, the lowest five states with $P=1$, the lowest four states with $P=2$, and the lowest two states with $P=3$, a total twenty-one vibrational states for each j. The total dimensionality was then $21 \times (j_{max}+1)$ or a total of 168 states when $j_{max}=7$. To verify convergence, additional test calculations were done in which the total number of rotational states included was *decreased* ($j_{max}=6$) while the number of CD states included in the contracted basis was *increased* to 29 (thirteen states with $P=0$, 7 states with $P=1$, six states with $P=2$, and three states with $P=1$. The calculated energies for *all* levels changed by less than 0.03 cm^{-1}.

Table VII presents a full comparison between the calculated vibration-rotation energies, as predicted by the adiabatic bender calculations discussed in the preceding section, those calculated within the centrifugal decoupling approximation (with a diagonal "coupled-states" centrifugal barrier [Eq. (21)] with $\bar{l}=1$), and the full CC energies for total angular momenta of $J=1$ and $J=5$. For $J=1$, the CC results presented were determined with the full, primitive basis and with the smaller contracted basis, discussed in the preceding paragraph. Although the latter might be expected to be deficient for the higher levels, we see that the difference between the calculated CC energies for $J=1$ is rarely larger than 0.3 cm^{-1}.

We observe first an extremely close agreement between the adiabatic bender and CD energies. The differences are always less than 1.5 cm^{-1}. This implies that the nonadiabatic corrections due to the crossings of the adiabatic curves in Figs. 7 and 9 are small. The excellent agreement between the adiabatic bender, CD, and CC energies clearly justifies the labelling of each level with the rotational parentage of a particular adiabatic bender potential and the stretch vibrational quantum number. In a similar spirit to this adiabatic model, an adiabatic bender approximation has found considerable utility for quantum scattering calculations of atom-diatom chemical reactions dominated by collinear geometries.[76,77] By assuming that the bending vibrational number is conserved in the reaction, considerable reduction in the computational overhead can be achieved.

The CD ($\bar{l}=1$) energies agree extremely well with the CC $J=1$ energies, which is further confirmation that P is a good quantum number for ArBH(A). In a few cases the shift between the CD and CC energies is greater than 1 cm^{-1}. In particular, consider the $P=1$ level labeled $j=1_u$, $v_s=2$ in Table VII ($E \approx -42$ cm^{-1}). Here the adiabatic and CD energies agree to within 0.7 cm^{-1}. Yet the CC energy for this level is lower by 2.5 cm^{-1}. Likely this, and the other relatively minor shifts, are a manifestation of Coriolis coupling, in particular between the handful of CD levels which lie within the range $-44 < E < -40$ cm^{-1}.

Within the adiabatic bender model, the Ar–BH motion is treated one dimensionally. For the calculated one-dimensional (in R) wave function one can calculate an effective ArBH rotational constant B, which is just proportional to $\langle R^{-2} \rangle$. Alternatively, one can use the results of the CC calculations for $J=1$ and 5 to determine an effective rotational constant, under the approximation that the shift between the $J=1$ and $J=5$ energies is equal to $B[J'(J'+1)-J(J+1)]$. The comparison between the ArBH(A) rotational constant, calculated from the adiabatic bender wavefunctions and from the J dependence of the CC energies, is made in Table VIII. The agreement is excellent for all levels lying below ~ -20 cm^{-1}, which lends further credence to the validity and usefulness of the adiabatic bender model.

VI. DISCUSSION

Figure 10 and Table VII illustrate the pattern of energy levels predicted for the ArBH(A) van der Waals molecule. Most distinct should be the relatively well separated levels with binding energies greater than 100 cm^{-1}. These correspond to two vibrational progressions (the $P=0$, $j=1_-$, $v_s=0-2$ levels and the $P=1$, $j=1_l$, $v_s=0-2$ levels) and the additional $P=2$, 2_l, $v_s=0$ level. As discussed in Sec. V A, these bender curves represent states governed primarily by the $V_{A''}$ PES. Further, in these states the BH moiety has, in the large-j limit, a helicopterlike internal motion, so that the internal rotation of the BH moiety is confined to a plane perpendicular to $\bar{R}$.

Unfortunately, as discussed in Sec. III, for the levels enumerated above we expect to observe only the $P=1$, 1_l, $v_s=0-2$ levels in the visible absorption spectrum of the vibrationally cold ArBH(X) complex near the BH($A\ ^1\Pi \leftarrow X\ ^1\Sigma^+$) transition. Since the minimum in the $P=1$, $j=1_l$ adiabatic bender curve occurs at smaller R than the minimum in the lowest ArBH(X) adiabat (see Fig. 9), we would anticipate that the spectra associated with these ArBH(A, $P=1$, $j=1_l$, v_s)$\leftarrow$ArBH(X, $P=0$, $v_s=0$) transitions will be blue degraded.

This article is copyrighted as indicated in the article. Reuse of AIP content is subject to the terms at: http://scitation.aip.org/termsconditions. Downloaded to IP: 128.114.34.22 On: Mon, 01 Dec 2014 02:28:08

TABLE VII. Calculated low-lying energy levels (in cm^{-1}) of the ArBH(A) complex, described by the modified PES's.

Adiabatic and CD ($\bar{l}=1$)												Full CC[a]					
$P=0$[b]				$P=1$[c]				$P=2$ and 3[c,d]				$J=1$[e]		$J=1$[f]		$J=5$[f]	
Adiab.	CD	j[g]	v_s[h]	Adiab.	CD	j[g]	v_s[h]	Adiab.	CD	j[g]	v_s[h]	$\pi=+1$	$\pi=-1$	$\pi=+1$	$\pi=-1$	$\pi=+1$	$\pi=-1$
−187.0	−187.9	1_-	0									−187.3		−187.2		−182.6	
				−174.0	−174.8	1_l	0					−174.4	−174.4	−174.3	−174.3	−169.7	−169.7
−140.9	−142.1	1_-	1									−141.6		−141.1		−136.7	
								−134.7	−134.7	2_l	0					−130.9	−130.9
				−128.9	−129.6	1_l	1					−129.2	−129.2	−128.7	−128.7	−124.5	−124.5
−101.7	−103.1	1_-	2									−102.6		−101.4		−97.2	
				−93.2	−94.5	1_l	2					−94.3	−94.3	−93.1	−93.1	−89.5	−89.5
								−88.1	−88.4	2_l	1					−84.3	−84.3
				−85.2	−84.7	1_u	0					−84.5	−84.5	−84.5	−84.5	−81.2	−81.2
−79.6	−80.3	2_-	0									−79.3		−79.3		−75.6	
								−69.8[d]	−69.7	3_l	0					−66.7	−66.7
−68.9	−70.4	1_-	3									−70.0		−67.9		−64.0	
				−64.6	−67.5	1_l	3					−67.2	−67.2	−65.8	−65.8	−62.0	−62.3
−63.4	−64.2	1_+	0										−64.0		−63.9		−61.0
				−62.1	−63.2	1_u	1					−62.8	−62.8	−62.8	−62.9	−59.6	−59.7
								−49.6	−49.9	2_l	2					−45.7	−45.7
				−45.8	−44.1	2_l	0					−45.4	−45.4	−45.2	−45.1	−42.6	−42.3
−44.5	−45.8	2_-	1									−45.0		−44.5		−41.1	
−42.8	−42.4	1_-	4									−43.3		−41.2		−37.6	
				−41.9	−41.2	1_u	2					−43.9	−43.8	−43.6	−43.6	−40.3	−40.7
−40.9	−43.8	1_+	1										−42.2		−42.2		−39.6
				−40.9		1_l	4					−40.9	−40.9	−39.3	−38.9	−35.7	−35.8
								−30.0	−28.6	2_u	0					−26.2	−26.2
				−25.0	−27.5	1_u	3					−27.2	−27.2	−27.2	−27.2	−24.8	−24.8
−23.2	−25.5	1_+	2										−25.3		−25.3		−23.1
				−22.4	−25.1	1_l	5					−24.9	−24.9	−23.3	−23.3	−20.5	−20.3
−22.9	−24.3	1_-	5									−23.9		−21.6		−18.4	
								−21.8[d]	−21.7	3_l	1					−18.3	−18.3
								−18.8	−19.1	2_l	3					−15.0	−16.0
−18.1	−17.8	2_+	0										−17.6		−17.6		−14.6
				−17.8	−17.5	2_u	0					−17.1	−16.8	−17.1	−16.8	−14.0	−13.1
−14.7	−15.9	2_-	2									−15.0		−15.0		−12.0	
				−13.6	−14.2	2_l	1					−14.0	−14.0	−14.0	−14.0	−11.8	−11.8
				−12.1	−11.8	1_u	4					−11.8	−11.7	−11.4	−11.8	−9.2	−9.3
−10.7	−10.3	1_+	3										−11.9		−11.4		−10.1
−9.1	−10.3	1_-	6									−10.1		−8.1		−6.0	
								−10.4	−10.7	2_u	0				−8.0	−8.0	
				−9.3	−10.2	1_l	6					−9.8	−9.8	−8.2	−8.2	−5.3	−5.3
				−3.7	−5.5	1_u	5					−5.4	−5.4	−5.4	−5.4	−3.9	−3.9
−3.0	−4.4	1_+	4										−4.3		−4.3		−3.0
				−1.7	−3.2	1_l	7					−3.2	−3.2	−2.3	−2.3	−0.7	−0.6
−1.4	−2.5	1_-	7									−2.4		−2.1		−0.01	
				[i]	−0.9							−0.8	−0.8	−0.8	−0.8		
[i]	−0.2												−0.2				

[a]The quantum number π designates the total parity of the vibration-rotation states.
[b]The states labeled + and − correspond, respectively, to $\epsilon=+1$ and -1, respectively [see the discussion after Eq. (13)]. All adiabatic curves (Fig. 9) for $P=0$ were diabatized.
[c]For $P>0$, the subscripts u and l designate the upper and the lower of the two adiabatic potentials which correlate with BH(j). The 1_l and 1_u curves were diabatized.
[d]The energies at −69.8 and −21.8, which correlate to the $j=3$ asymptote, correspond to $P=3$. All other energies correspond to $P=2$.
[e]Full distributed Gaussian basis.
[f]Contracted basis built out of lowest CD states expanded in distributed Gaussian basis.
[g]Correlation between the particular adiabatic bender potential and the asymptotic rotational quantum number of the separated BH molecule in the $A\ ^1\Pi$ state (see Fig. 9).
[h]van der Waals stretching quantum number.
[i]Adiabatic bender states at these energies were not found.

At higher energy will appear additional levels corresponding to higher stretch states of the $P=0$, $j=1_-$ and $P=1$, $j=1_l$ and 2_l adiabatic bender curves, as well as other levels associated with the $P=0$, $j=2_-$ and 1_+, and $P=1$, $j=1_u$ and 2_l adiabatic bender curves. Since the minima in these curves occur at larger R, beyond the minimum in the ArBH(X) adiabat (see Fig. 9), we would anticipate that the spectra associated with transitions to these higher levels will

This article is copyrighted as indicated in the article. Reuse of AIP content is subject to the terms at: http://scitation.aip.org/termsconditions. Downloaded to IP:

TABLE VIII. Comparison of ArBH(A) rotational constants (in cm^{-1}) calculated within the adiabatic bend-stretch approximation and from full close-coupled calculations.

Adiabatic[a]								CC
$P=0$[b]				$P=1$[c]				
E[e]	B[f]	j[g]	v_s[h]	E[e]	B[f]	j[g]	v_s[h]	B_{eff}[d]
−187.0	0.1643	1_-	0					0.168
				−174.0	0.1643	1_l	0	0.164
−140.9	0.1534	1_-	1					0.157
				−128.9	0.1516	1_l	1	0.150
−101.7	0.1414	1_-	2					0.138
				−93.2	0.1360	1_l	2	0.139
				−85.2	0.1168	1_u	0	0.119
−79.6	0.1351	2_-	0					0.132
−68.9	0.1281	1_-	3					0.124
				−64.6	0.1231	1_l	3	0.131
−63.4	0.0978	1_+	0					0.105
				−62.1	0.1197	1_u	1	0.114
				−45.8	0.1129	2_l	0	0.098
−44.5	0.1270	2_-	1					0.121
−42.8	0.1134	1_-	4					0.129
				−41.9	0.1019	1_u	2	0.122
−40.9	0.0887	1_+	1					0.113
				−40.9	0.1093	1_l	4	0.127
				−25.0	0.0887	1_u	3	0.086
−23.2	0.0777	1_+	2					0.077
				−22.4	0.0938	1_l	5	0.103
−22.9	0.0970	1_-	5					0.111
−18.1	0.0966	2_+	0					0.107
				−17.8	0.1010	2_u	0	0.121
−14.7	0.1161	2_-	2					0.105
				−13.6	0.1035	2_l	1	0.077
				−12.1	0.0746	1_u	4	0.084
−10.7	0.0664	1_+	3					0.045
−9.1	0.0772	1_-	6					0.076
				−9.3	0.0757	1_l	6	0.104
				−3.7	0.0560	1_u	5	0.055
−3.0		1_+	4					0.048
				−1.7	0.0519	1_l	7	0.063
−1.4	0.0514	1^-	7					0.075

[a]All adiabatic bender curves (see Fig. 9) were diabatized (see text).
[b]The states labeled + and − correspond, respectively, to $\epsilon=+$ and -1, respectively [see the discussion after Eq. (13)].
[c]The subscripts u and l designate the upper and the lower of the two adiabatic potentials which correlate with BH(j).
[d]Effective rotational constant, obtained from shift in the calculated energies for $J=5$ vs $J=1$.
[e]Energies of adiabatic bend-stretch levels; see Table VII.
[f]Rotational constant for adiabatic bend-stretch levels, computed from the expectation value of R^{-2}.
[g]Correlation between the adiabatic bender curve supporting this level and the asymptotic rotational quantum number of the separated BH($A\ ^1\Pi$) molecule.
[h]van der Waals stretch vibrational quantum number.

display *red* degraded bands. As discussed in Sec. III, if the rotational motion of the BH moiety is not significantly hindered in the ArBH complex, we would anticipate that the Franck–Condon factors will be weak for transitions out of the lowest ArBH(X) level to levels associated with ArBH(A) adiabats which correlate asymptotically with BH(A) rotor levels with $j>1$.

Aside from this qualitative prediction, we have calculated Franck–Condon factors only for transitions from the lowest ArBH(X) level to the ArBH(A) $P=1$, $j=1_l$, $v_s=0-2$ levels (see the following article[21]), in order to compare with the relative experimental intensities in this progression. Because of the transition from the free rotor limit to a hindered rotor with decreasing R, we find that the overlap integrals involving the van der Waals stretch coordinate only are not an accurate measure of the band intensities. An eventual comparison of theoretical and experimental intensities would provide a further test of the accuracy of the modified *ab initio* PES's. Franck–Condon factors, or vibrational band strengths, can be calculated readily from the variational wavefunctions for the bend-stretch levels. Within the adiabatic bender model, the Franck–Condon factors are proportional to averages, over the one-dimensional stretching wave functions, of the overlap between the *eigen*vectors of the $T(R)$ matrix of Eq. (14) which correspond to the initial and final states.

This article is copyrighted as indicated in the article. Reuse of AIP content is subject to the terms at: http://scitation.aip.org/termsconditions. Downloaded to IP: 128.114.34.22 On: Mon, 01 Dec 2014 02:28:03

A more detailed comparison with experiment is the subject of the following article.[21] As will be seen, with the help of the theoretical predictions represented by Table VI it is possible to assign unambiguously the first ten experimentally observed bands in the visible $\tilde{A}\leftarrow\tilde{X}$ absorption spectrum of the ArBH van der Waals complex. This comparison, and the assignment of the spectra which would have not been possible without the input of the theoretical investigation presented here, underscores the power of a joint theoretical experimental investigation.

In addition to presenting the results of sophisticated multireference, configuration-interaction calculations which provided the template for the ArBH(X,A) PES's, our work has illustrated the usefulness of the adiabatic bender model. Here, the two-dimensional ArBH PES's are prediagonalized in the bending degree of freedom, which then provides a one-dimensional potential for the assignment and *quantitative* determination of the stretch-bend energies of the ArBH complex. Indeed, the slight errors in the adiabatic bender energies, when compared to more exact calculations based on the same PES's, are far less than the uncertainties in these PES's due to limitations in the treatment of dynamic electron correlation in our *ab initio* calculations. Notwithstanding, the comparison with experiment to be presented in the following article, shows clearly that with only a slight modification of the *ab initio* PES's, which preserves the qualitative aspects of these PES's, one can accurately predict and, more importantly, *assign* the experimentally observed spectra of the ArBH van der Waals complex.

Note added in proof. The concept of a Born–Oppenheimer separation of radial and angular motion in a van der Waals complex was first developed by Holmgren, Waldman, and Klemperer.[78]

ACKNOWLEDGMENTS

M. H. A. and P. J. D. wish to thank the U. S. Air Force Office of Scientific Research and the National Science Foundation for support of the research reported here under Grant Nos. AFOSR-91-0363 and CHE-92223081, respectively, and Marsha Lester for her continued encouragement. The participation of S. G. was made possible by support of the DoD AASERT award program. Some of the calculations reported here were supported by a grant of HPC time on the CRAY YMP-8 and C916 systems at the DoD HPC Shared Resource Center, U.S. Army Corp of Engineers Waterways Experiment Station, Vicksburg, MI.

APPENDIX: THE BF→SF TRANSFORMATION

The BF→SF transformation given by Eq. (8) is identical to that given earlier by Kouri, Heil, and Shimoni.[79] The phase factor differs from that given by Hutson[29] in that the projection quantum number P enters in with a *positive* sign. The correctness of the sign given in Eq. (8), which may be important in cases involving diatomic molecules with even spin multiplicity, can be demonstrated as follows:

The angular basis functions which appear on the right-hand side of Eq. (3) can be written as[39]

$$D^{j*}_{m_j,\Lambda}(\alpha,\beta,0)=\sum_P D^{j*}_{m_j,P}(\hat{R})D^{j*}_{P,\Lambda}(\hat{r}_b), \tag{A1}$$

where the angles are defined in Sec. II. After introduction of Eq. (A1) into Eq. (2), the product of the two functions of $\hat{R}$ [$Y_{lm_l}(\hat{R})$ and $D^{j*}_{m_j,P}(\hat{R})$] can be reexpressed as a single rotation matrix element:

$$Y_{lm_l}(\hat{R})D^{j*}_{m_j,P}(\hat{R})$$
$$=\left(\frac{2l+1}{4\pi}\right)^{1/2}\sum_C(2C+1)\begin{pmatrix} j & l & C\\ m & m_l & c\end{pmatrix}$$
$$\times\begin{pmatrix} j & l & C\\ P & 0 & c'\end{pmatrix}D^C_{c,c'}(\hat{R}), \tag{A2}$$

where $c=-m-m_l$ and $c'=-P$. The sum over m and m_l in Eq. (2) can be eliminated using the orthogonality of the $3j$ symbols. This imposes $C=J$. We consequently find

$$\sum_{m_jm_l}(jm_jlm_l|JM)Y_{lm_l}(\hat{R})D^{j*}_{m_j,\Lambda}(\alpha,\beta,0)$$
$$=\sum_P(2J+1)^{1/2}(-1)^{j-l+P}\begin{pmatrix} j & l & J\\ P & 0 & -P\end{pmatrix}D^{j*}_{P,\Lambda}(\hat{r}_b), \tag{A3}$$

which, after taking the inverse transformation, leads to Eq. (8).

[1] For a good recent review, see M. C. Heaven, J. Phys. Chem. **97**, 8567 (1993).
[2] W. Meyer, Int. J. Quant. Chem. Symp. **5**, 341 (1971).
[3] W. Meyer, J. Chem. Phys. **58**, 1017 (1973).
[4] A. Degli-Esposti and H.-J. Werner, J. Chem. Phys. **93**, 3351 (1990).
[5] M. T. Berry, M. R. Brustein, J. R. Adamo, and M. I. Lester, J. Phys. Chem. **92**, 5551 (1988).
[6] M. T. Berry, M. R. Brustein, and M. I. Lester, J. Chem. Phys. **90**, 5878 (1989).
[7] W. M. Fawzy and M. C. Heaven, J. Chem. Phys. **89**, 7030 (1988); **92**, 909 (1990).
[8] B.-C. Chang, L. Yu, D. Cullin, B. Rehfuss, J. Williamson, T. A. Miller, W. M. Fawzy, X. Zheng, S. Fei, and M. Heaven, J. Chem. Phys. **95**, 7086 (1991).
[9] M. T. Berry, M. R. Brustein, M. I. Lester, C. Chakravarty, and D. C. Clary, Chem. Phys. Lett. **178**, 301 (1991).
[10] M. I. Lester, R. W. Randall, L. C. Giancarlo, and S. E. Choi, J. Chem. Phys. **99**, 6211 (1993).
[11] W. H. Green, Jr., and M. I. Lester, J. Chem. Phys. **96**, 2573 (1992).
[12] M. I. Lester, W. H. Green, Jr., C. Chakravarty, and D. C. Clary, in *Molecular Dynamics and Spectroscopy by Stimulated Emission Pumping*, edited by H.-L. Dai and R. W. Field (World Scientific, New York, 1993).
[13] M.-L. Dubernet and J. H. Hutson, J. Chem. Phys. **99**, 7477 (1993).
[14] J. M. Bowman, B. Gazdy, P. Schafer, and M. C. Heaven, J. Phys. Chem. **94**, 2226 (1990); **94**, 8858 (1990).
[15] U. Schnupf, J. M. Bowman, and M. C. Heaven, Chem. Phys. Lett. **189**, 487 (1992).
[16] M. I. Lester, R. A. Loomis, L. C. Giancarlo, M. T. Berry, C. Chakravarty, and D. C. Clary, J. Chem. Phys. **98**, 9320 (1993).
[17] R. W. Randall, C.-C. Chuang, and M. I. Lester, Chem. Phys. Lett. **200**, 113 (1993).
[18] G. Jansen and B. A. Hess, Chem. Phys. Lett. **192**, 21 (1992).
[19] M. H. Alexander, P.-J. Dagdigian, and H.-J. Werner (unpublished).
[20] G. W. Lemire, M. J. McQuaid, A. J. Kotlar, and R. C. Sausa, J. Chem. Phys. **99**, 91 (1993).
[21] E. Hwang and P. J. Dagdigian, following paper, J. Chem. Phys. **101**, 2903 (1994).

This article is copyrighted as indicated in the article. Reuse of AIP content is subject to the terms at: http://scitation.aip.org/termsconditions. Downloaded to IP:

[22] W. M. Fawzy, G. T. Fraser, J. T. Hougen, and A. S. Pine, J. Chem. Phys. **93**, 2992 (1990).
[23] M.-L. Dubernet, D. Flower, and J. M. Hutson, J. Chem. Phys. **94**, 7602 (1991).
[24] M.-L. Dubernet, P. A. Tuckey, and J. M. Hutson, Chem. Phys. Lett. **193**, 355 (1992).
[25] J. Tennyson and A. van der Avoird, J. Chem. Phys. **77**, 5664 (1984).
[26] J. M. Hutson, J. Chem. Phys. **89**, 4550 (1988).
[27] B. P. Reid, K. C. Janda, and N. Halberstadt, J. Phys. Chem. **92**, 587 (1988).
[28] D. C. Clary and D. J. Nesbitt, J. Chem. Phys. **90**, 7000 (1989).
[29] J. M. Hutson, in *Advances in Molecular Vibrations and Collision Dynamics*, edited by J. M. Bowman and M. A. Ratner (JAI, Greenwich, CT, 1991) Vol. 1A, p. 1.
[30] K. Bergmann and W. Demtröder, Z. Phys. **243**, 1 (1971).
[31] H. Klar, J. Phys. B **6**, 2139 (1973).
[32] G. C. Nielson, G. A. Parker, and R. T Pack, J. Chem. Phys. **66**, 1396 (1977).
[33] S. Green and R. N. Zare, Chem. Phys. **7**, 62 (1975).
[34] M. H. Alexander, J. Chem. Phys. **76**, 5974 (1982).
[35] M. H. Alexander, Chem. Phys. **92**, 337 (1985).
[36] D. Lemoine, G. C. Corey, M. H. Alexander, and J. Derouard, Chem. Phys. **118**, 357 (1987).
[37] D. G. Sauder, D. Patel-Misra, and P. J. Dagdigian, J. Chem. Phys. **91**, 5316 (1989).
[38] J. M. Brown, J. T. Hougen, K.-P. Huber, J. W. C. Johns, I. Kopp, H. Lefebvre-Brion, A. J. Merer, D. A. Ramsay, J. Rostas, and R. N. Zare, J. Mol. Spectrosc. **55**, 500 (1975).
[39] D. M. Brink and G. R. Satchler, *Angular Momentum*, 2nd ed. (Clarendon, Oxford, 1968).
[40] M. H. Alexander, H.-J. Werner, and P. J. Dagdigian, J. Chem. Phys. **89**, 1388 (1988).
[41] R. N. Zare, *Angular Momentum* (Wiley, New York, 1988).
[42] A. Arthurs and A. Dalgarno, Proc. R. Soc. London Ser. A **256**, 540 (1960).
[43] C. F. Curtiss and F. T. Adler, J. Chem. Phys. **20**, 249 (1952).
[44] P. McGuire and D. J. Kouri, J. Chem. Phys. **60**, 2488 (1974).
[45] R. T Pack, J. Chem. Phys. **60**, 633 (1974).
[46] J. Tennyson and B. T. Sutcliff, J. Chem. Phys. **77**, 4061 (1982).
[47] C. Chakravarty and D. Clary, J. Chem. Phys. **94**, 4149 (1991).
[48] T. H. Dunning, Jr., J. Chem. Phys. **90**, 1007 (1989).
[49] R. A. Kendall, T. H. Dunning, Jr., and R. J. Harrison, J. Chem. Phys. **96**, 6796 (1992).
[50] MOLPRO is a package of *ab initio* programs written by H.-J. Werner and P. J. Knowles, with contributions from J. Almlöf, R. Amos, S. Elbert, K. Hampel, W. Meyer, K. Peterson, E. A. Reinsch, R. Pitzer, M. Deegan, A. Stone, and P. Taylor.
[51] K. P. Huber and G. Herzberg, *Molecular Spectra and Molecular Structure. IV. Constants of Diatomic Molecules* (Van Nostrand Reinhold, New York, 1979).
[52] S. F. Boys and F. Benardi, Mol. Phys. **19**, 553 (1970).
[53] H.-J. Werner and P. J. Knowles, J. Chem. Phys. **82**, 5053 (1985).
[54] P. J. Knowles and H.-J. Werner, Chem. Phys. Lett. **115**, 259 (1985).
[55] P. J. Knowles and H.-J. Werner, Chem. Phys. Lett. **145**, 514 (1988).
[56] H.-J. Werner and P. J. Knowles, J. Chem. Phys. **89**, 5803 (1988).
[57] H.-J. Werner and W. Meyer, J. Chem. Phys. **74**, 5794 (1981).
[58] R. N. Diffenderfer and D. R. Yarkony, J. Phys. Chem. **86**, 5098 (1982).
[59] B. H. Lengsfield, J. Chem. Phys. **77**, 4073 (1982).
[60] H.-J. Werner and P. J. Knowles, Theor. Chim. Acta **78**, 175 (1990).
[61] E. R. Davidson and D. W. Silver, Chem. Phys. Lett. **53**, 403 (1977).
[62] R. J. Gadnitz and R. Alrichs, Chem. Phys. Lett. **143**, 413 (1988).
[63] W. Meyer, Theoret. Chim. Acta **35**, 277 (1974).
[64] C. Hampel, K. Peterson, and H.-J. Werner, Chem. Phys. Lett. **190**, 1 (1992), and references contained therein.
[65] M. J. O. Deegan and P. J. Knowles (unpublished).
[66] Tables of the *ab initio* energies and the expansion coefficients in Eq. (18), as well as a FORTRAN program to determine the radial expansion coefficients $V_\lambda(R)$ in the expansion of V_{sum} and V_{dif} as a function of R are available on request from mha by electronic mail (address: mha@hibridon.umd.edu). Please supply a return electronic mail address.
[67] E. Hwang, Y.-L. Huang, P. J. Dagdigian, and M. H. Alexander, J. Chem. Phys. **98**, 8484 (1993).
[68] J. M. Parson, P. E. Siska, and Y. T. Lee, J. Chem. Phys. **56**, 1511 (1972).
[69] D. J. Kouri, in *Atom-Molecule Collision Theory: A Guide for the Experimentalist*, edited by R. B. Bernstein (Plenum, New York, 1979), p. 301.
[70] W. T. M. L. Fernando and P. F. Bernath, J. Mol. Spectrosc. **145**, 392 (1991).
[71] HIBRIDON is a package of programs for the time-independent quantum treatment of inelastic collisions and photodissociation written by M. H. Alexander, D. E. Manolopoulos, H.-J. Werner, and B. Follmeg, with contributions by P. F. Vohralik, D. Lemoine, G. Corey, B. Johnson, T. Orlikowski, W. Kearney, A. Berning, A. Degli-Esposti, C. Rist, and P. Dagdigian.
[72] G. Herzberg, *Spectra of Diatomic Molecules*, 2nd Ed. (Van Nostrand, Princeton, 1968).
[73] G. Herzberg, *Molecular Spectra and Molecular Structure III, Electronic Spectra and Electronic Structure of Polyatomic Molecules* (Van Nostrand, Princeton, 1967).
[74] S. Fei, X. Zhang, and M. C. Heaven, J. Chem. Phys. **97**, 1655 (1992).
[75] I. P. Hamilton and J. C. Light, J. Chem. Phys. **84**, 306 (1986).
[76] J. M. Bowman, Adv. Chem. Phys. **61**, 115 (1985).
[77] Q. Sun, J. M. Bowman, G. C. Schatz, J. R. Sharp, and J. N. L. Connor, J. Chem. Phys. **92**, 1677 (1990).
[78] S. L. Holmgren, M. Waldman, and W. Klemperer, J. Chem. Phys. **67**, 4414 (1977).
[79] D. J. Kouri, T. G. Heil, and Y. Shimoni, J. Chem. Phys. **65**, 226 (1976).

This article is copyrighted as indicated in the article. Reuse of AIP content is subject to the terms at: http://scitation.aip.org/termsconditions. Downloaded to IP: